

1 **Aerosol-CFD modelling of ultrafine and black carbon particle emission,**
2 **dilution, and growth near roadways**

3
4 Li Huang*, Sunling Gong**

5 Previously at Air Quality Research Division, Atmospheric Science and Technology
6 Branch, Environment Canada, Toronto, Ontario, Canada.

7 * now at Environmental Monitoring and Reporting Branch, Ontario Ministry of the Environment and
8 Climate Change
9 125 Resources Rd
10 Toronto M9P 3V6, Ontario, Canada
11 **now at Chinese Academy of Meteorological Sciences
12 46 Zhong-Guan-Cun S. Ave.
13 Beijing 100081, CHINA
14

15
16 Mark Gordon, John Liggio, Ralf Staebler, Craig A. Stroud, Gang Lu, Cristian Mihele,
17 Jeffrey R. Brook

18
19 Air Quality Research Division, Atmospheric Science and Technology Branch,
20 Environment Canada, Toronto, Ontario, Canada.

21
22 Charles Q. Jia
23
24 Department of Chemical Engineering and Applied Chemistry,
25 University of Toronto, Toronto, Ontario, Canada.

26
27

1 **Abstract**

2 Many studies have shown that on-road vehicle emissions are the dominant source of
3 ultrafine particles (UFP; diameter < 100 nm) in urban areas and near-roadway
4 environments. In order to advance our knowledge on the complex interactions and
5 competition among atmospheric dilution, dispersion and dynamics of UFPs, an aerosol
6 dynamics-CFD coupled model is developed and validated against field measurements. A
7 unique approach of applying periodic boundary conditions is proposed to model pollutant
8 dispersion and dynamics in one unified domain from the tailpipe level to the ambient
9 near-road environment. This approach significantly reduces the size of the computational
10 domain, and therefore, allows fast simulation of multiple scenarios. The model is
11 validated against measured turbulent kinetic energy (TKE) and pollution horizontal
12 gradients perpendicular to a major highway. Through a model sensitivity analysis, the
13 relative importance of individual aerosol dynamical processes on the total particle
14 number concentration (N) and particle number-size distribution (PSD) near a highway is
15 investigated. The results demonstrate that (1) coagulation has a negligible effect on N and
16 particle growth, (2) binary homogeneous nucleation (BHN) of H₂SO₄-H₂O is likely
17 responsible for elevated N closest to the road, (3) N and particle growth are very sensitive
18 to the condensation of semi-volatile organics (SVOCs), particle dry deposition, and the
19 interaction between these processes. The results also indicate that, without the proper
20 treatment of atmospheric boundary layer (i.e. its wind profile and turbulence quantities),
21 the nucleation rate would be underestimated by a factor of 5 in the vehicle wake region
22 due to overestimated dilution. Therefore, introducing ABL conditions to activity-based

- 1 emission models may potentially improve their performance in estimating UFP traffic
- 2 emissions.

1

2 **1. Introduction**

3 Many studies have shown that vehicle emissions are the dominant source of ultrafine
4 particles (UFP; diameter < 100 nm) in urban areas and near-roadway environments. For
5 example, about 95% of UFP (diameter = 50~100 nm) observed near a US freeway were
6 apportioned to fresh vehicular emissions (Toner et al., 2008). In the more confined
7 environment of a street canyon, over 99% of particles in number were found to be below
8 300 nm and number concentrations of particles in this size range were found to be
9 linearly correlated with the traffic volume (Kumar et al., 2008). Due to their small size
10 and abundance in number, recent toxicological and epidemiological studies suggest a
11 strong correlation between adverse health effects and personal exposure to UFPs (e.g.
12 (Brugge et al., 2007;Ruckerl et al., 2007;Valavanidis et al., 2008)). A recent review study
13 by Schlesinger (2007) pointed out that the health impacts of chemical constituents, such
14 as sulphate, seem to be inconsistent across all epidemiological studies. Comparing
15 epidemiological studies of heart rate variability in humans, Grahame (2009) suggests that
16 differences in accuracy of exposure information for health-relevant emissions may
17 explain conflicting study results. This has led to an urgent need to study the temporal and
18 spatial variations of local traffic emission in the vicinity of roadways.

19 With the growing concern of adverse health effects from exposure to UFPs, the gradients
20 of vehicle-emitted pollutants (such as CO, NO_x, and UFPs) have been measured in the
21 ambient atmosphere near roadways (e.g. (Beckerman et al., 2008;Reponen et al.,
22 2003;Pirjola et al., 2006;Zhu et al., 2009)). For example, Zhu et al. (2009) found that
23 elevated particle numbers decay exponentially on the downwind side of three different

1 types of roadways with increasing distance and reach background levels within a few
2 hundred meters. Karner et al. (2010) synthesized field measurements of near-roadway
3 pollutants from over 40 monitoring studies and investigated the concentration-distance
4 relationship. The variation of UFP concentrations near roadways among studies is likely
5 affected by factors including meteorological conditions (wind speed, ambient
6 temperature, relative humidity, and atmospheric stability), traffic characteristics (volume
7 and fleet composition), the geometry of roadways, and aerosol transformation processes
8 (nucleation, coagulation, condensation/evaporation, and dry deposition). However, field
9 measurements alone are often associated with such limitations as low spatial or temporal
10 resolution in sampling, conclusions restricted by local meteorology, and difficulties in
11 separating the effects of interactive processes.

12 Therefore, numerical modelling of UFPs has been conducted to address these limitations.
13 Due to the challenge of resolving processes with very different scales, a two-stage
14 dilution modelling strategy, including ‘tailpipe-to-road’ and ‘road-to-ambient’ dilutions,
15 has been proposed (Zhang and Wexler, 2004; Zhang et al., 2004). In the first stage (i.e.
16 ‘tailpipe-to-road’), strong vehicle induced turbulence (VIT) results in fast and strong
17 dilution (dilution ratio ~ 1000 in 1 s) and triggers nucleation and
18 condensation/evaporation. While in the ‘road-to-ambient’ stage, atmospheric boundary
19 layer turbulence (ABLT) continues to dilute exhaust particles with ambient air
20 accompanied with particle size changes due to condensation/evaporation. A review study
21 by Carpentieri et al. (2011) has shown that, with recent advances in numerical modelling,
22 computational fluid dynamics (CFD) models can be valuable tools for nanoparticle
23 dispersion in the first stage of dilution. In addition to the limited spatial scale of the

1 dispersion investigated, other limitations in these most recent modelling studies include
2 PSD and chemical composition not being explicitly resolved (Chan et al., 2010). Recent
3 modelling studies of UFP dispersion on street level, on the other hand, have crudely
4 simplified treatment of vehicular emission, VIT and aerosol dynamics (Gidhagen et al.,
5 2004a;Gidhagen et al., 2003;Kumar et al., 2009).

6 Most recently, Wang et al. (2013) proposed a two-stage simulation approach to integrate
7 the “tailpipe-to-road” dispersion into the “road-to-ambient” dispersion stage for the first
8 time. As the authors noted, however, the proposed approach remains computationally
9 demanding, especially when both particle size and chemical composition need to be
10 resolved. To effectively model UFP dynamics and dispersion near roadways in a single
11 unified ‘tailpipe-to-ambient’ domain, a unique approach of applying periodic boundary
12 conditions to the computational domain is proposed in this paper. Compared to a ‘road-
13 to-ambient’ dispersion modelling approach, the advantage of a unified domain is that the
14 uncertainty due to a simplified or non-existent treatment of VIT can be greatly reduced
15 by explicitly modelling VIT. With VIT being explicitly modelled, aerosol dynamics
16 (such as nucleation, condensation and evaporation) triggered by the rapid first-stage
17 dilution can be properly incorporated into dispersion models to study their effects on
18 roadside air quality. From a modelling perspective, such a unified model provides a tool
19 to link individual tailpipe emissions (controlled laboratory measurements) to roadside air
20 quality (ambient field measurements), which is a noted challenging task (Keskinen and
21 Ronkko, 2010). As the main focus of this paper, we present the development and
22 validation of a multi-component sectional aerosol dynamics-CFD coupled model to

1 account for the complex dilution, dispersion and dynamics of UFPs immediately after
2 tailpipe emission to ambient background.

3

4 **2. Aerosol dynamics-CFD coupled model**

5 **2.1. Multiphase approach to the mixture of atmospheric gas and aerosol**

6 Following previous studies (e.g. (Li et al., 2006b;Uhrner et al., 2007;Wang et al.,
7 2013;Albriet et al., 2010)), the commercial CFD code ANSYS FLUENT is used to model
8 turbulent flow around realistically-shaped vehicles. An Euler-Euler approach to
9 multiphase atmospheric air flow is coupled with new particle formation, transformation
10 and dry deposition processes. Among the general multiphase models available in
11 FLUENT, the mixture multiphase model is chosen for the present work due to its
12 superior numerical efficiency compared to the Eulerian multiphase model (ANSYS,
13 2009a). The concept of “phase” in the FLUENT multiphase model is defined in a broad
14 sense as an identifiable class of material that has a particular inertial response to and
15 interaction with the flow (ANSYS, 2009b). The gas phase and the particulate phase in the
16 real atmosphere are represented in the model by the “primary phase” and a number of
17 “secondary phases”, respectively. The number of “secondary phases” is determined by
18 the number of discrete size bins used to resolve the particle number-size distribution. The
19 flow field of the “mixture phase” is obtained by numerically solving Reynolds-averaged
20 Navier-Stokes equations (RANS) including conservation equations of mass, momentum
21 and energy with the standard k- ϵ turbulence model.

22 For the transport of gas and particulate species, FLUENT predicts the local mass fraction
23 of each species by solving the advection-diffusion equations. The volume fraction of each

1 secondary phase in a control volume (equivalent to the number concentration of particles
2 of the same size) is obtained by numerically solving the continuity equation for the
3 secondary phase with a specified source term due to aerosol dynamic processes. The
4 diffusive mass flux in FLUENT is modelled as the sum of two components: molecular
5 and turbulent diffusion (e.g. Eq. 4 in (Di Sabatino et al., 2007)). Turbulent diffusion due
6 to VIT and ABLT are the main dilution mechanisms for pollutants in the near-road
7 environment (Zhang and Wexler, 2004). The key parameter governing modelled
8 turbulent diffusion of pollutants using the RANS approach is the turbulent Schmidt
9 number (Sc_t), which is defined as the ratio of the turbulent momentum diffusivity and the
10 turbulent mass diffusivity. Analyzing a widely distributed range of Sc_t (0.2-1.3) in
11 literature versus the commonly used values (0.7-0.9), Tominaga and Stathopoulos (2007)
12 found that, for plume dispersion in open country for example, a smaller value of Sc_t
13 might be used to compensate the underestimated turbulent momentum diffusion. They
14 further suggested to adopt its “standard” value in simulations without this type of
15 underestimation. Therefore, given the successful model validation on TKE (discussed in
16 Section 4.1.1), the standard value of 0.7 for Sc_t is used in our study. Thus, the advection,
17 the turbulent mixing, and the diffusion of gases and particles are inherently treated by
18 FLUENT through the continuity equation for each phase. Aerosol dynamic processes,
19 which change the chemical components in particle and gas phases, are integrated through
20 the source terms in continuity equations, and incorporated into FLUENT through User-
21 Defined Functions (UDF).

22

23 **2.2. Aerosol dynamics**

1 Each secondary phase is a particulate phase composed of mixed chemical components
 2 within a specified size range. The density of particles in a given size bin is dynamically
 3 computed by FLUENT based on the volume-weighted mixing law. From the continuity
 4 equation for each secondary phase p , the volume fraction of the secondary phase (α_p) is
 5 obtained by solving

$$6 \quad \frac{\partial}{\partial t}(\alpha_p \rho_p) + \nabla \cdot (\alpha_p \rho_p \overline{u_m}) = -\nabla \cdot (\alpha_p \rho_p \overline{u_{dr,p}}) + S_\alpha, \quad (1)$$

7 where $\overline{u_{dr,p}}$ is the drift velocity of secondary phase, and S_α is the source of mass transfer
 8 due to aerosol dynamic processes. Number concentration of particles in size bin p (N_p , in
 9 particles/cm³) is computed from the ratio of the phase volume fraction solved by
 10 FLUENT to the particle volume of a certain size:

$$11 \quad N_p = 10^{-6} \cdot \frac{\alpha_p}{(4/3)\pi(D_p/2)^3}, \quad (2)$$

12 where D_p is the diameter (in m) for particles in size bin p . And the local mass
 13 concentration of chemical component i from particles in size bin p is calculated from the
 14 phase volume fraction (α_p) and the local mass fraction (Y_i) as:

$$15 \quad m_i = 10^9 \cdot \alpha_p \rho_p Y_i. \quad (3)$$

16 The underlying implementation of aerosol dynamics is a multi-component, size-resolved,
 17 sectional aerosol model, as described as follows.

18 **2.2.1. Nucleation**

19 Immediately after tailpipe emissions, new particles form by homogeneous nucleation
 20 with initial particle size around 1.5-2.0 nm in the first few milliseconds of exhaust
 21 cooling and dilution (Kulmala et al., 2007). A qualitative investigation by Zhang and

1 Wexler (2004) found that sulphuric acid-induced nucleation could be the dominant new
2 particle production process. The experimental study conducted by Arnold et al. (2006)
3 observed a positive correlation between gaseous sulphuric acid and particle number in the
4 exhaust of a passenger diesel car burning ultra-low sulphur fuel, indicating an important
5 role of sulphuric acid-induced nucleation. The sulphuric acid gas emission rate is
6 estimated based on fuel sulphur content following Uhrner et al. (2007). The
7 parameterization of BHN of H₂SO₄-H₂O (Vehkamaki et al., 2003) developed specifically
8 for engine exhaust dilution conditions is implemented in this study. This parameterization
9 has already been successfully used in a number of different aerosol-CFD applications
10 (e.g. (Uhrner et al., 2007;Uhrner et al., 2011;Albriet et al., 2010;Wang and Zhang,
11 2012)).

12 **2.2.2. Coagulation**

13 Particles in the exhaust plume collide due to random (Brownian) motion and turbulent
14 mixing to form larger particles, which is called coagulation. The coagulation process
15 reduces N (mainly in the smaller size range) while preserving the aerosol total mass.
16 However, it modifies the particle number size distribution, and internally mixes particles
17 of different chemical composition over the population. Coagulation may be driven by
18 Brownian motion, turbulent flow conditions, gravitational collection, inertial motion and
19 turbulent shear respectively. Individual coagulation rate coefficients (or coagulation
20 kernels) due to the above driving forces are calculated in this work based upon Jacobson
21 (2005), with consideration of particle flow regimes and convective Brownian diffusion
22 enhancement. The overall coagulation rate coefficient is the summation of individual
23 coefficients.

1 **2.2.3. Condensation and evaporation**

2 A complex mixture of condensable gases, including water vapor, sulphuric acid and
3 semi-volatile organics (SVOCs), is emitted from the tailpipe after fuel combustion in the
4 engine. During the strong dilution and cooling stage of up to a few seconds after emission
5 (Zhang and Wexler, 2004), supersaturation of these condensable gases occurs and favors
6 the diffusion-limited mass transfer process from the gas phase to the pre-existing particle
7 phase. Following primary emission and nucleation, condensation of SVOCs was
8 suggested by a number of studies (e.g. (Clements et al., 2009; Wang and Zhang,
9 2012; Albriet et al., 2010; Uhrner et al., 2011; Mathis et al., 2004)) to be responsible for the
10 rapid growth of nanoparticles in the exhaust plume. As the reverse of condensation,
11 evaporation occurs due to further dilution of condensable gases to subsaturation level in
12 the air surrounding exhaust particles. It was suggested by field measurements of freeway
13 emissions from predominantly gasoline vehicles that lower ambient temperature may
14 favor the condensation of organic species to the particle phase (Kuhn et al., 2005). In this
15 study, the net mass transfer rate of a condensable gas from/to an existing particle with
16 multiple components is driven by the difference between the bulk partial pressure and the
17 saturation vapor pressure above the particle surface (Jacobson, 2005). The calculation of
18 mass transfer rate implements corrections to the diffusion coefficient, the thermal
19 conductivity of air, and the saturation vapor pressure over curved particle surfaces to
20 reflect its dependence on particle size and chemical composition.

21 **2.2.4. Dry deposition**

22 Driven by mechanisms such as Brownian diffusion, turbulent diffusion, sedimentation,
23 and advection, dry deposition removes particles at the air-surface interface when they

1 contact and remain on the surface (Jacobson, 2005). Brownian diffusion is more effective
2 in removing smaller particles due to their larger diffusion coefficient, while
3 sedimentation is more important for larger particles whose fall speeds are much higher. In
4 the current study, parameterization of particle dry deposition follows the size-resolved
5 dry deposition scheme developed by Zhang et al. (2001). The effect of turbulent mixing
6 on particle dry deposition is taken into account by the locally calculated friction velocity.
7 This parameterization has been successfully validated and implemented in a number of
8 air quality and climate studies (e.g. (Gong et al., 2003;Pye and Seinfeld, 2010)), and it
9 has recently been improved and extended (Petroff and Zhang, 2010). The recent
10 development accounts for more detailed characteristics of the surface canopy, and
11 suggests possible overestimation of dry deposition velocity for particles in the fine mode.
12 Thus, our current study is likely biased to overestimate the removal of UFPs by dry
13 deposition.

14

15 **2.3. Modelling turbulence**

16 For turbulence modelling, although the large eddy simulation (LES) approach has been
17 reported to be a more promising solution, the standard k- ϵ turbulence model is
18 implemented in this work for several reasons. First, the high computational demands of
19 the LES approach prevent its application for modelling the dispersion and transformation
20 of multiple pollutants with complex geometry (i.e. gas and particle emissions and aerosol
21 dynamics from multiple vehicles in this study). Compared to RANS closures, the LES
22 approach is at least one order of magnitude more computationally expensive (Rodi,
23 1997). Secondly, a proper treatment of the atmospheric boundary layer (ABL) has proven

1 to be crucial to dispersion modelling studies (Blocken et al., 2007b;Zhang, 1994). Recent
2 advances made by (Balogh et al., 2012;Parente et al., 2011a, b) permit a general and
3 practical means to include the ABL using the standard k- ϵ model. To achieve this in LES
4 simulations, on the other hand, inflow conditions would have to be carefully generated
5 with additional, significant computational overhead (Xie and Castro, 2008;Li et al.,
6 2006b). Finally, RANS models agree reasonably well with experimental data in
7 predicting mean flow and pollutant concentrations (e.g. (Labovsky and Jelemensky,
8 2011;Sklavounos and Rigas, 2004)). Kim et al. (2001) successfully modelled the
9 dispersion of a truck exhaust plume in a wind tunnel using k- ϵ turbulent closure focusing
10 on rapid dilution and turbulent mixing of exhaust CO₂.

11 Although CFD codes have been widely adopted in pollutant dispersion modelling, the
12 accuracy of such simulations can be seriously compromised when wall functions based
13 on experimental data for sand-grain roughened pipes and channels are applied at the
14 bottom of the computational domain (Blocken et al., 2007b;Riddle et al., 2004). Attempts
15 have been made to better predict ABL flow by changing turbulent model constants,
16 tuning boundary profiles, and modifying wall functions and turbulent transport equations
17 (Blocken et al., 2007a;Pontiggia et al., 2009;Li et al., 2006a;Alinot and Masson,
18 2005;Hargreaves and Wright, 2007;Labovsky and Jelemensky, 2011;Balogh et al.,
19 2012;Parente et al., 2011a, b). Among the aforementioned studies, recent advances made
20 by Balogh et al. (2012) and (Parente et al., 2011a, b) are implemented in this work, which
21 permits a general and practical means to include ABL using the standard k- ϵ model in the
22 CFD code, FLUENT. The ABL profiles of mean velocity, TKE, and dissipation rate for
23 atmospheric flow under neutral stratification conditions (Richards and Hoxey, 1993) are:

$$1 \quad u = \frac{u^*}{\kappa} \ln\left(\frac{z + z_0}{z_0}\right) \quad (4)$$

$$2 \quad k = \frac{u^{*2}}{\sqrt{C_\mu}} \quad (5)$$

$$3 \quad \varepsilon = \frac{u^{*3}}{\kappa(z + z_0)} \quad (6)$$

4 A modified wall function for turbulent mean velocity following (Parente et al., 2011b):

$$5 \quad u = \frac{u^*}{\kappa} \ln(E'z^{+'}) \quad (7)$$

6 is implemented through UDF and applied to wall adjacent cells, where $E' = \frac{\nu}{z_0 u^*}$ and

7 $z^{+'} = \frac{(z + z_0)u^*}{\nu}$. To keep the default constant value of σ_ε in the standard k- ε model, a

8 source term is added to the dissipation rate equation as follows:

$$9 \quad S_\varepsilon(z) = \frac{\rho_m u^{*4}}{(z + z_0)^2} \left(\frac{(C_2 - C_1)\sqrt{C_\mu}}{\kappa^2} - \frac{1}{\sigma_\varepsilon} \right). \quad (8)$$

10 Furthermore, we adopt the approach by Parente et al. (2011a) to allow a gradual
 11 transition from Eq. (4-6) (i.e the undisturbed ABL) to the wake region simulated by the
 12 standard k- ε model (Supplement, S4).

13

14 **3. Simulation setup**

15 **3.1. FEVER field study**

16 The Fast Evolution of Vehicle Emissions from Roadway (FEVER) study was conducted
 17 to monitor pollutant gradients perpendicular to a major highway north of Toronto,
 18 Canada (Hwy-400; 43.994 N, 79.583 W). The model developed and tested in this paper

1 was designed to simulate the FEVER observations. A complete description of the
2 monitoring strategies of the FEVER project were documented in (Gordon et al.,
3 2012a; Gordon et al., 2012b), the BC emission rate for gasoline vehicles was estimated by
4 Liggio et al. (2012), and the rapid organic aerosol production under intense solar
5 radiation was investigated by Stroud et al. (2014).

6 The site under investigation was a 6-lane (25 m across from the lane edges) highway,
7 mainly surrounded by flat agricultural fields and some trees lining the side roads, with
8 negligible local pollution sources other than vehicular emissions. To validate modelled
9 VIT, the on-road TKE data measured by the Canadian Regional and Urban Investigation
10 System for Environmental Research (CRUISER) mobile laboratory were compared with
11 modelled TKE. The on-road TKE data was measured by two 3D sonic anemometers
12 during passenger vehicle chasing experiments on six days between 20 August and 15
13 September 2010. To validate modelled near road dispersion, a case study period of 14
14 and 15 September 2010 between 05:00-08:00 a.m. EDT was chosen for comparison. The
15 near-road TKE data was measured by a 3D sonic anemometer at a 3-m tower located 22
16 m east of the road centre. Wind speed and direction data was measured by an AirPointer
17 system (Recordum GmbH), averaged every minute, 34 m east of the road centre. As
18 shown in Table 1, the predominant wind direction was approximately perpendicular to
19 the highway and the median Monin-Obukhov length indicates near neutral stability
20 conditions. The CRUISER mobile lab housed instrumentation to measure BC, CO₂, and
21 UFP while driving transects perpendicular to the highway. Following a previous study
22 (Gordon et al., 2012a), data were filtered for winds within 45° of the highway normal,
23 which results in removing less than 5% of the data. In addition, particle size distributions

1 between 14.6 and 661.2 nm were measured at two fixed sites with an SMPS every 3
2 minutes and averaged for 05:00-06:00 and 06:00-08:00 a.m. of 14 and 15 September
3 2010 for model validation.

4 **3.2. Computational domain and flow boundary conditions**

5 The sizes of computational domain used for near road dispersion modelling in this study
6 are summarized in Table 2. The computation domain for the base case simulation, for
7 example, is shown in Fig. 1a. The top of the domain is set to 50 m above ground so that
8 the turbulent flow near the surface is not affected by the top boundary (the x-y plane in
9 purple mesh). The horizontal dimension of 375 m perpendicular to the highway (x-axis)
10 is determined by considering the availability of measurements and the extent of pollutant
11 dispersion (Gordon et al., 2012a). Both dimensions of the domain are in compliance with
12 the recommendations for CFD simulation of flows in the urban environment (Franke,
13 2007). To reduce computational overhead, first, the actual two-way, 6-lane traffic fleet is
14 represented by a one-way, 3-lane traffic fleet (as shown in Fig. 1b) while conserving the
15 total traffic volume; Then, translational periodic boundary conditions are applied to the x-
16 z planes (in Cyan mesh) to account for the effects of the stable, continuous traffic fleet on
17 the highway by numerically repeating the computational domain in the direction of y-
18 axis. Based on the measured traffic volume of about 104.3 passenger vehicles/min,
19 travelling speed of approximately 120 km/hr (or 33.3 m/s), and the assumed average
20 vehicle length of 4.5 m, the average y-axis distance (bumper to bumper) between two
21 vehicles travelling in adjacent lanes is calculated as 11.5 m assuming all 3 lanes are
22 evenly occupied. Thus, the horizontal dimension of 48 m along the highway (y-axis) is
23 calculated based on the measured traffic volume for weekday early morning rush hours

1 between 06:00-08:00 a.m. The whole domain is meshed into 871,065 unstructured
2 hexahedral cells with the finest ones concentrated around the moving vehicles, tailpipes,
3 and their wake regions and immaterially above the ground.

4 In our simulation, the vehicles are set to be stationary, nonslip walls with a roughness
5 length of 0.0015 m (Wang and Zhang, 2009), while the blowing air has two velocity
6 components: the first component towards the vehicles (or the negative y-axis direction) of
7 33.3 m/s in magnitude; and the second component perpendicular to the highway (or the
8 negative x-axis direction) in a form given by Eq. (4). The first component of wind
9 velocity accounts for the relative movement between the moving vehicles and still air,
10 and the second component describes the observed wind speed according to a fully
11 developed ABL wind profile under neutral stratification. Thus, the upwind side boundary
12 parallel to the road (the x-y plane in purple mesh) and the top boundary are set as velocity
13 inlets. The ground surface is set to have the same velocity magnitude as the running
14 vehicles but in the opposite direction. The modified wall function (Eq. 7) and the
15 additional source term to dissipation rate (Eq. 8) as described in Section 2.3 are applied to
16 the ground surface to account for a fully developed ABL turbulent flow. Translational
17 periodic boundary conditions are set to the x-z planes of the domain, and a pressure outlet
18 boundary is applied to the boundary (in red mesh) at the far end side to the highway.

19 Each tailpipe, 52 mm in diameter, is specified as mass flow inlet with a mass flow rate of
20 0.055 kg/s and an exhaust temperature of 480 K (Uhrner et al., 2007). An O-Grid
21 composed of 7 inflation layers, whose thickness gradually increase from 0.003 m, around
22 vehicles is used to allow the standard wall functions to apply to the fully-turbulent layer
23 around moving vehicles. Crucial but not mentioned in previous CFD models, a high

1 spatial resolution applied here results in a dimensionless wall distance ($y^+ = \rho\mu_t y / \mu$)
2 of about 90 at the vehicle surface, which is well within the suggested range of 30 to 300
3 for the standard wall functions to apply (ANSYS, 2009b). Simulation results of
4 turbulence and pollutant concentrations at Site B (33 m east of the Hwy centre) show no
5 significant dependence on a further refined grid (Supplement, S2).

6

7 **3.3. Chemical boundary conditions: background concentrations and traffic**

8 **emissions**

9 In addition to meteorological and traffic data, chemical data of gases and particles are
10 required as part of CFD boundary conditions. According to the source type, the required
11 chemical data are divided into two categories: background concentrations and traffic
12 emission rates. The mass concentrations of background gaseous and particulate species
13 from the FEVER field measurements are listed in Table 3, with their corresponding
14 values used as model input. The background gas phase includes dry air (O_2 and N_2),
15 water vapor and CO_2 . The CO_2 volume fraction and RH value are converted to mass
16 fractions to specify the species input values for the velocity inlet boundaries. For the
17 particulate phase, a bi-modal log-normal particle size distribution is assumed (as
18 summarized in Table 5). The parameters of background particles are obtained from the
19 FEVER measurements at about 100 m upwind of Hwy-400. Given the total background
20 N and PSD, the volume fractions of individual size bins are obtained, and the mass of
21 black carbon (BC) and organic aerosol (OA) are distributed into each size bin according
22 to the ratio of their background mass concentrations listed in Table 3.

1 Vehicles driving on the highway continuously emit a complex mixture of gases and
2 particles. It is not possible to include a complete set of gaseous and particulate species in
3 the model, which also is not numerically practical. In this study, the tailpipe emission
4 rates of the gaseous and particulate species are summarized in Table 4. Currently, the
5 exhaust gas is composed of CO₂, H₂O, H₂SO₄, SVOCs, and N₂, which are key species to
6 the aerosol dynamics and dispersion. The treatment of H₂SO₄ as direct emission rather
7 than a mixture of SO₂ and SO₃ followed by hydrolysis has been explained in Section
8 2.2.1. It was suggested by modelling single exhaust plumes (e.g. (Albriet et al.,
9 2010;Uhrner et al., 2007;Uhrner et al., 2011)) that SVOCs are likely to be responsible for
10 the rapid growth in particle size when they condense on UFPs. Following Albriet et al.
11 (2010), pyrene (C₁₆H₁₀), n-nonadecane (C₁₉H₄₀), and n-pentacosane (C₂₅H₅₂) are
12 introduced to represent the polycyclic semi-volatile organic compounds, the semi-volatile
13 alkanes between C₁₄ and C₂₂, and semi-volatile alkanes between C₂₃ and C₂₉,
14 respectively. The mass fractions of the above three groups of SVOCs are based on
15 Albriet et al. (2010), and the total mass emission rate of SVOCs is set as 0.0186 g/km
16 (Pye and Seinfeld, 2010). All SVOCs initially from the tailpipe are assumed to exist only
17 in the gas phase, but are subject to interactions with the particle phase through
18 condensation/evaporation upon immediate dilution with the surrounding air. To reduce
19 the number of species considered in the model, the non-volatile fraction of primary
20 organic aerosol (POA) from tailpipes is assumed to share the properties of the
21 background OA, i.e. with an average molecular mass of 300 g/mol and an average
22 density of 1.5 g/cm³. This assumption is not likely to affect our results because the
23 amount of the non-volatile fraction of POA from tailpipes is very small compared to the

1 background OA. N and PSD for tailpipe emissions are based on a recent study by
2 Nikolova et al. (2011b), which provides an emission rate according to traffic volume and
3 type. As pointed out by Nikolova et al. (2011a), however, their original proposed
4 parameterization implicitly accounts for fast nucleation process. As indicated by
5 laboratory measurements (Ronkko et al., 2007; Kirchner et al., 2009), the nucleation mode
6 particles have a nonvolatile core in the exhaust of a heavy duty diesel vehicle; however,
7 they are completely volatile under 280 °C in the exhaust of a diesel passenger car. Thus,
8 we assume in this study that N of nucleation mode particles from all passenger cars are
9 from BHN, while those from heavy duty vehicles have a solid core of BC and nonvolatile
10 POA. Given the mass flow rate of the tailpipe exhaust, the mass fraction of each
11 individual species can be estimated from its mass emission rate listed in Table 4. These
12 mass fractions are used to specify chemical boundary conditions for tailpipes.

13

14 **4. Results and Discussions**

15 Turbulent mixing of tailpipe emissions with the ambient air largely determines the initial
16 dilution and the three-dimensional distribution of the traffic pollutants downwind of
17 roadways. Thus, the modelled TKE is first compared against on-road and near-road TKE
18 measurements reported by Gordon et al. (2012b). For model validation results in Section
19 4.1, two scenarios with different traffic conditions (base case: 06:00-08:00 a.m. and half
20 traffic case: 05:00-06:00 a.m.) are considered. The modelled CO₂ and BC concentrations
21 and PSDs are compared with the FEVER field measurements. Finally, the impacts of
22 individual aerosol dynamical processes on UFPs and model sensitivity to the treatment of
23 ABL are investigated in Section 4.2. A total of 5 sensitivity runs are performed based

1 upon the base case (06:00-08:00 a.m.). Four sensitivity runs are conducted by turning off
2 a single aerosol dynamical process for each run, and the results are compared with the
3 base case in Table 6. An additional sensitivity run is conducted without maintaining
4 modelled ABL profiles through Eqs. (7-8).

6 **4.1 Model validation**

7 **4.1.1 Turbulent kinetic energy**

8 Both theoretical (e.g. (Zhang and Wexler, 2004;Ketzler and Berkowicz, 2004)) and
9 monitoring (e.g. (Zhou and Levy, 2007)) studies have concluded that dilution is the
10 dominant mechanism governing N of UFPs. And the turbulent kinetic energy (TKE)
11 measures the strength of mixing and dilution. Figure 2 compares the modelled TKE with
12 the measurements from the FEVER chasing experiments of passenger cars on highways.
13 The x-axis in Fig. 2 is the following time behind passenger cars and the y-axis is 10-s
14 average TKE. The modelled TKE values in Fig. 2 are calculated for individual vehicle
15 wakes super-imposed on an estimated background on-road TKE of $2.4 \text{ m}^2/\text{s}^2$ (Gordon et
16 al., 2012b). The average travelling speed during the FEVER chasing experiments was
17 about 20 m/s, and 84.5% of the measurements were taken at a chasing speed between 15
18 and 25 m/s. Therefore, model simulations are conducted for passenger cars travelling at
19 15, 20, and 25 m/s. As shown in Fig. 2, the modelled TKE in the wake of a vehicle
20 travelling at speed of 15-25 m/s agrees well within the 25th and 75th percentile of the
21 measurements. And the variations among modelled TKE in Fig. 2 show the sensitivity of
22 on-road TKE to vehicle type and travelling speed. With these scenarios agreeing within

1 the 25th and 75th percentile of the measurements, it is clear that the turbulent mixing
2 within individual vehicle wakes on the highway can be reasonably well modelled.
3 As a measure of the turbulent dilution under perpendicular wind conditions, near-road
4 TKE is also modelled and compared to the measurements at a tower located 22 m east of
5 the road centre. Two time periods (05:00-06:00 and 06:00-08:00 a.m.) with distinctly
6 different traffic volumes are considered. For both time periods, the atmospheric boundary
7 layer was neutrally stratified. The average traffic volume, however, increased from 54.9
8 to 104.3 vehicles per minute, as shown in Fig. 2 of (Gordon et al., 2012a). Although the
9 tower is stationary, the distance and time along the wind trajectory from the highway
10 centre vary with changing wind direction and speed. Therefore, the evolution of
11 turbulence with distance can be investigated based on measurements at a fixed location in
12 a Lagrangian sense. There are 120 and 240 measurements of TKE taken for the periods of
13 05:00-06:00 and 06:00-08:00 a.m., respectively, and they are binned by distance as
14 shown in Fig. 3. The obtained wind trajectory distances vary between 20 to 80 m with
15 about 93% of them concentrating on the first bin (20-40 m). For the period of 05:00-
16 06:00 a.m., the measured (modelled) TKE at a distance of 20-40 m from the highway
17 centre is in the range of 0.46-0.80 (0.58-0.73) m^2/s^2 . Similarly, for the period of 06:00-
18 08:00 a.m., the measured (modelled) TKE lies in the range of 0.55-0.90 (0.65-0.95)
19 m^2/s^2 . Although the observed TKE decay is limited in spatial resolution for both time
20 periods, the comparison in Fig. 3 shows an adequate agreement with the field
21 measurements and suggests turbulent mixing in a roadside environment can be
22 successfully modelled even with varying traffic volumes.

23 **4.1.2 Near-road concentration gradients: CO₂ and BC**

1 As a chemically passive gas species in vehicular emissions, CO₂ is an ideal indicator of
2 atmospheric mixing of tailpipe exhaust with ambient air. In a previous study (Kim et al.,
3 2001), CO₂ was experimentally measured inside a single turbulent plume of heavy-duty
4 truck exhaust and successfully modelled with the standard k-ε model in the CFD code
5 FLUENT. The focus of this study, however, is the horizontal concentration gradient on
6 the downwind side of a highway.

7 Fig. 4(a) shows the concentration of CO₂ (ppmv) as a function of downwind distance
8 from the centre of Hwy-400 for the morning period of 06:00-08:00 a.m. FEVER
9 measurements were first corrected to wind trajectory distance, grouped into 20 m bins
10 between 50 and 350 m, and then plotted in median concentrations and 25th and 75th
11 percentiles. Modelled CO₂ concentrations closely follow the decreasing trend of the
12 median values of the FEVER measurements, and agree well within the 25th and 75th
13 percentiles. However, the model tends to underestimate CO₂ concentrations by about 6
14 ppmv in the first 50 m (i.e. 50-100 m) of downwind distance and overestimate by about 8
15 ppmv in the last 50 m (i.e. 250-300 m). Similarly, the concentration-distance relationship
16 for particulate BC is shown in Fig. 4(b). Modelled BC concentrations are also within the
17 25th and 75th percentiles exhibiting a trend with distance similar to the median of the
18 measured values. Similar to CO₂, minor underestimations (15%) between 50-100 m from
19 Hwy-400 and slight overestimations (20%) after 100 m were observed for particulate BC.
20 This behavior of the model suggests slightly overestimated pollutant concentrations
21 between 0-3 m above the ground within 100 m distance to the road, possibly due to
22 underestimated vertical mixing by the model. Beyond 100 m away from the road, vertical
23 diffusion of the near surface pollutants results in the overestimations. There are two

1 factors that may explain the underestimated vertical mixing closest to the road. Firstly,
2 the modelled road structure is missing a 1-m-high barrier at the highway centre, which
3 could potentially lift near surface pollutants under cross wind conditions (Ning et al.,
4 2010;Hagler et al., 2011). Secondly, midsize and heavy-duty trucks are neglected due to
5 their small fractions in total traffic, which emit pollutants at a greater height up to 4 m
6 than 0.5 m for passenger cars (Gordon et al., 2012a).

7

8 **4.1.3 Particle size distribution**

9 The fate of atmospheric particles depends strongly on PSD, which is the result of the
10 complex influences of mobile emissions, atmospheric dilution and transformation
11 processes. In Fig. 5, the predicted PSDs are compared to SMPS measurements for two
12 selected periods of the early morning rush hours (i.e. 05:00-06:00 and 06:00-08:00 a.m.)
13 at two fixed locations: Sites B and C, located 34 and 300 m from Hwy-400, respectively.
14 The early morning rush hours are subdivided into the above two periods based on hourly
15 averaged traffic flow. According to Gordon et al. (2012a), the traffic flow of 06:00-08:00
16 a.m. (105 veh/min) almost doubled the average traffic of 05:00-06:00 a.m. (55 veh/min),
17 while the ambient conditions (such as atmospheric stability class, incoming solar
18 radiation, and wind velocity) remained approximately constant.

19 Comparing the measured PSDs at two sites, it was found that for all measured particle
20 sizes, the number concentrations decreased significantly when particles were transported
21 from 34 to 300 m downwind of the highway. The observed total particle number
22 concentrations decreased by a factor of about 2.5 and 5.7 between these two locations for
23 the periods of 05:00-06:00 and 06:00-08:00 a.m., respectively. Similar to many previous

1 roadside monitoring studies reviewed by Pant and Harrison (2013), the measured PSDs
2 showed distinct multi-modal size regimes (i.e. nucleation, soot and accumulation modes)
3 in the measured size range of 15-700 nm. Tri-modal lognormal curve fitting of the
4 observed PSDs revealed a nucleation mode at 20-25 nm, a soot mode at 65-75 nm and an
5 accumulation mode at 160-380 nm. In agreement with (Zhu et al., 2002b;Zhu et al.,
6 2002a), the nucleation mode particles dominated N and decreased much faster (by a
7 factor of 8 in this study) than that of the accumulation particles (only a factor of 2 in this
8 study). It was also found that the geometric mean diameter of the nucleation mode
9 increased from 20.0 (at Site B) to 24.7 nm (at Site C), which may be attributed to the
10 condensation of SVOCs (Clements et al., 2009) and the coagulation of nucleation mode
11 particles (Zhu et al., 2002b).

12 The comparison in Fig. 5 demonstrates an adequate agreement between the modelled and
13 the observed PSD at both distances under different traffic conditions. For the peak traffic
14 hours during 06:00-08:00 a.m., the model estimated total particle number concentrations
15 are 6.25×10^4 and 1.66×10^4 particles/cm³ at Sites B and C, respectively with
16 approximately 10% underestimations compared to the observations. Secondly, the
17 dominant nucleation mode was properly captured by the current model, as well as its
18 decreasing trend with increasing distance from the highway. Furthermore, the nucleation
19 mode particles were modelled to grow from 19.8 to 24.3 nm in geometric mean diameter
20 with increasing distance away from the highway. This agrees exceptionally well with the
21 observations. Similar conclusions can be drawn from the 05:00-06:00 a.m. comparison.
22 However, the model clearly underestimated the number concentrations of particles of
23 100-730 nm in diameter. This discrepancy can be attributed, at least partially, to the

1 missing non-tailpipe emissions in the current model, such as brake wear, road-tyre
2 interaction and re-suspension of road dust as reviewed by Kumar et al. (2013). Although
3 road dust particles formed mechanically by frictional contact between road surface and
4 tire or between break system components are assumed to be primarily coarse particles,
5 both laboratory experiments (Dahl et al., 2006; Gustafsson et al., 2008) and real-world
6 measurements (Mathissen et al., 2011) recently observed a significant portion of particles
7 of 6-700 nm in diameter. On the other hand, the estimated emission factors for sub-
8 micrometer particles generated by the road-tire interaction under steady driving condition
9 based on these studies vary significantly, indicating that the emission strength tends to be
10 very site specific. Thus, the underestimated particles larger than 100 nm might be a result
11 of missing estimates of non-tailpipe emissions for the underlying site.

12

13 **4.2 Model sensitivity analysis**

14 **4.2.1 Role of aerosol dynamical processes**

15 Along with dilution, aerosol dynamical processes (i.e. condensation/evaporation,
16 coagulation, nucleation, and dry deposition) may interact with one another and modify N
17 and PSD in near-road environments. In this section, the relative importance of the above
18 aerosol dynamical processes is investigated by conducting simulations with individual
19 processes removed and comparing against the base case simulation, in which all
20 dynamical processes are considered by the model. The obtained N and the geometric
21 mean diameter of nucleation mode particles from this sensitivity analysis are summarized
22 in Table 6. The base case simulation demonstrates that in moving from Site B to Site C,
23 the nucleation mode particles decreases by approximately a factor of 3, and the

1 geometric-mean diameter increases by 4.5 nm. The modelled soot mode and
2 accumulation mode particles are excluded from the analysis due to significant
3 underestimations compared to the measurements, as discussed in the previous section.
4 The results of excluding particle dry deposition process are investigated first because its
5 impact on N can interact with particle nucleation and condensation processes, as
6 discussed later in this section.

7 When particle dry deposition is deactivated in the model, nucleation mode particle
8 numbers increase significantly (~ 23 and 53% at Site B and C, respectively), resulting in
9 1-5 nm smaller geometric mean diameters compared to the base case as listed in Table 6.

10 The modelled particle dry deposition velocity is up to 0.2 m/s for the smallest particles of
11 3-5 nm in diameter due to strong Brownian diffusion. Our results show that particle dry
12 deposition plays a significant role in governing N in the vicinity of roadways between 30
13 and 300 m. Gidhagen et al. (2004b) estimated that dry deposition removes only about
14 12% of total particles near a Swedish highway, in contrast to our estimation of 15-35%.

15 This discrepancy may be due to the different treatment of atmospheric boundary layer
16 turbulence in both studies. Gidhagen et al. (2004b) introduced an artificial source of
17 turbulence into their model to mimic the observed atmospheric dilution of NO_x near the
18 road, while the theoretically- based method by Parente et al. (2011b) combined with the
19 measured ABLT was implemented in this study. The modelled VIT and ABLT have been
20 validated against the measurements in Section 4.1.1.

21 Compared with the base case simulation, the predicted mean diameters at both sites
22 without condensation remain nearly unchanged from the tailpipe emission of 15 nm. At
23 the same time, the predicted particle number concentrations without condensation are

1 about 1 order of magnitude lower than the base case, and are the lowest among all
2 scenarios. The implication of this is two-fold. In agreement with previous modelling
3 studies (i.e.(Wang and Zhang, 2012;Uhrner et al., 2007;Uhrner et al., 2011;Albriet et al.,
4 2010)), it strongly suggests that the condensation of SVOCs is responsible for the growth
5 of nucleation mode particles during their atmospheric transport. It also reflects the strong
6 interactions between particle growth and removal processes in governing the simulated
7 particle number. Without the condensational growth of nucleation mode particles, new
8 particles formed due to the BHN mechanism remains in the smallest size bin of 3-5 nm in
9 diameter. Immediately after formation, these particles are subject to efficient removal by
10 dry deposition due to their small particle sizes, resulting in the lowest N among scenarios.
11 This result implies that controlling tailpipe SVOC emissions may indirectly help reduce
12 UFP number concentrations in the vicinity of roadways.

13 For the scenario without BHN of H₂SO₄-H₂O, the geometric mean diameters at both sites
14 are similar to the base case with slightly more condensational growth in size. However,
15 the particle number concentrations are underestimated by 36 and 10% at Site B and C,
16 respectively, compared to the base case. This implies that over 60 and 90% of the
17 nucleation mode particles at Site B and C are attributed to HDV emissions with non-
18 volatile cores. The result also shows that the BHN of H₂SO₄-H₂O has the greatest impact
19 on the particle population closest to the road. This is because the particles formed through
20 BHN are much smaller in size than those directly emitted with non-volatile cores around
21 15 nm in diameter. Thus, particles of BHN origins are subject to faster dry deposition
22 removal, and contribute less to N at greater distances in the near-road environment.

1 However, it should not be ignored in air quality modelling studies of mobile emissions,
2 especially within the first 100 m of the roadways.

3 The scenario excluding particle coagulation alone results in the least impact on both N
4 and geometric mean diameter of nucleation mode particles near the road. The results
5 strongly agree with both timescale analysis (Zhang and Wexler, 2004) and previous CFD
6 modelling studies (Wang and Zhang, 2012; Albriet et al., 2010; Gidhagen et al., 2004b).

7 However, the coagulation process was suggested to be important under mild to weak
8 atmospheric dilution conditions, such as street canyons (Gidhagen et al., 2004a) and road
9 tunnels (Gidhagen et al., 2003).

10 **4.2.2 Role of atmospheric boundary layer**

11 Previous studies have shown that accurate CFD simulation of the ABL (including its
12 wind profile and turbulence quantities) is essential for atmospheric dispersion of inert
13 pollutants. For example, Gorle et al. (2009) investigated the effect of atmospheric TKE
14 on the dispersion of particles of 1 μm in diameter, and concluded the impact was
15 significant. In their study, however, aerosol dynamical processes were not considered,
16 nor were their interactions with the ABLT. Here, a sensitivity analysis on the ABL is
17 performed to investigate the impact of the ABL on UFP formation and dispersion in the
18 near roadway environment. Specifically, the base case simulation is compared with a test
19 simulation where only the wall-function modifications of Eqs. (7-8) are not applied.

20 Figure 6a shows the model predicted UFP concentrations of the base case and the test
21 simulations, along with the integration of SMPS data at two fixed locations for the 06:00-
22 08:00 a.m. morning rush hours. The predicted concentrations of UFPs from the test
23 simulation are lower by about 1×10^4 particles/cm³ (or 18% of the background corrected

1 peak concentration) near the centre of the highway compared to the base case. However,
2 the concentration difference for CO₂ (as shown in Fig. 6b) between the two simulations is
3 only slightly different (~ 10% of its background corrected peak value). The
4 underestimated concentrations of both pollutants are due to unrealistic acceleration of the
5 surface wind and changes in the TKE profile in the upstream region of the computational
6 domain, as discussed in (Blocken et al., 2007b). Thus, the concentration underestimation
7 for CO₂ is the result of the overestimated dilution near the surface, where vehicular
8 exhaust occurs.

9 In addition to the overestimated dilution effect on particle dispersion, the impact of the
10 ABL on UFP number concentrations is enhanced by the reduced nucleation rate due to
11 the underestimation of gaseous precursors (i.e. H₂SO₄ and H₂O) in the vehicle wake
12 regions. The maximum nucleation rate from both simulations is around 2.9×10^{16}
13 particles/m³/s, which are in the range of $1 \sim 6.3 \times 10^{16}$ particles/m³/s from single vehicle
14 exhaust plume simulations (Wang and Zhang, 2012; Uhrner et al., 2007). Although the
15 maximum nucleation rate is not sensitive to ABL profiles, the area averaged nucleation
16 rate of the cross-section in the exhaust pipe plane behind the vehicle is underestimated by
17 a factor of 5 due to the overestimated dilution behind vehicles in the sensitivity run. This
18 comparison strongly suggests that the concentration of UFPs from mobile sources may be
19 even more sensitive to the ABL conditions than inert gaseous species. It also implies that
20 introducing ABL conditions to activity-based emission models (such as (Nikolova et al.,
21 2011b)) may potentially improve their performance in estimating UFP traffic emissions.

22

23 **5. Conclusions**

1 In this study, an aerosol dynamics-CFD coupled model is applied to a single unified
2 computational domain to investigate the dynamics and dispersion of UFPs from tailpipe
3 exhaust to the near-road environment. The interactions among individual exhaust plumes
4 are explicitly modelled within the “tailpipe-to-ambient” computational domain. The
5 unique application of translational periodic boundary conditions effectively reduces the
6 size of the computational domain and allows fast multiple-scenario simulations of size-
7 and chemical component-resolved aerosol dynamics. This paper has demonstrated that,
8 together with field measurements, the model is an effective tool which can be used to
9 advance our knowledge on the formation and dispersion of UFPs in the near-road
10 environment. This information is needed to help develop parameterizations of sub-grid
11 processes ultimately to improve air quality model simulations over urban areas.

12 The model was successfully validated with FEVER field study measurements of both on-
13 road and near-road TKE. The results indicate that the strength of turbulent mixing of
14 pollutants due to VIT and the ABLT is properly captured by the model, leading to good
15 agreements between modelled and measured concentrations for CO₂ and BC. For UFPs,
16 the modelled PSDs demonstrated adequate agreement with measurements at two fixed
17 locations near a major highway, under different traffic conditions. Sensitivity analysis
18 indicated that the modelled N and PSD of UFPs are sensitive to H₂SO₄-H₂O binary
19 homogeneous nucleation, condensation/evaporation of SVOCs, and particle dry
20 deposition. However, for such an unconfined near-road environment as in this study,
21 coagulation appears to have negligible effect on UFPs. Results also suggest that UFPs
22 from mobile sources may be even more sensitive to ABL conditions than inert species
23 because the average nucleation rate in vehicle wakes is very sensitive to the dilution of

1 H₂SO₄. Therefore, introducing ABL conditions to activity-based emission models may
2 potentially improve their performance in estimating UFP traffic emissions.
3 The next step of our study is to conduct multiple-scenario simulations and to provide
4 parameterizations on mobile emissions to large scale air quality models. Ultimately, a
5 unified model of UFP dynamics and dispersion can help predict exposures in the vicinity
6 of roadways to support risk assessments and health effect studies. Better treatment of
7 these processes in air quality models is also expected to allow for more accurate
8 predictions of the impacts specific vehicle emission control strategies may have on near-
9 road air quality and subsequent health and environmental benefits.

10

11 **Glossary**

12	u	ABL mean velocity
13	k	Turbulent kinetic energy or TKE
14	ε	Dissipation rate of TKE
15	u^*	Friction velocity
16	κ	Von Karman constant
17	z	Height above the ground
18	z_0	Aerodynamic roughness length
19	C_μ	Constant in the standard k- ε model
20	σ_ε	Turbulent Prandtl number for ε
21	E'	Wall function constant
22	$z^{+'}$	Non-dimensional wall distance
23	ν	Kinematic viscosity

1

2 **Acknowledgements**

3 This research was supported through the Program of Energy Research and Development
4 (PERD) under the specific Particle and Related Emission projects C11.008 and C12.007.
5 PERD is a program administered by Natural Resources Canada. The authors would also
6 like to thank Professor Alessandro Parente at Université Libre de Bruxelles and his
7 colleagues for providing CFD code for modelling the ABL in FLUENT.

1

2 **Tables and Figures**

3 Table 1. Median values of the measured meteorological data and model input.

Background PM	FEVER measured value	Model input
Relative humidity	86.5%	87%
Ambient temperature (K)	283.65	283.15
3-m wind speed (m/s)	1.4	1.4
3-m wind direction (degree)	264	260
Friction velocity (m/s)	0.3	0.3
Monin-Obukhov length (m)	36.9	N/A

4

5 Table 2. Domain sizes for near road dispersion simulations under different traffic flow
6 conditions.

Scenario	Case study period (EDT)	Domain dimensions (x-y-z)
Base case and sensitivity runs	06:00-08:00 a.m.	375 m×48 m×50 m
Half traffic case	05:00-06:00 a.m.	375 m×91 m×50 m

7

8 Table 3. Background concentrations of particulate and gaseous species considered in the
9 model.

Background PM	FEVER measured value	Model input
BC ($\mu\text{g}/\text{m}^3$)	0.298-0.53	0.39
OA ($\mu\text{g}/\text{m}^3$)	0.676-1.50	1.04
PM _{2.5} ($\mu\text{g}/\text{m}^3$)	~5.0	4.78
N ($\#/ \text{cm}^3$)	4921-7335	5800
CO ₂ (ppmv)	412.7-421.3	415

10

1

2 Table 4. Tailpipe gaseous and particulate species mass emission rates (g/km driven) for

3 gasoline engines. *Canada's National Inventory Report 1990-2009.

Species	Reference emission rates (g/km driven)	Reference	Model input (g/km driven)
CO ₂	278	Estimated from fuel-based emission factors * and the observed vehicle composition	278
SVOCs	0.0186	Gasoline powered vehicles (Pye and Seinfeld, 2010)	0.0186
H ₂ SO ₄	2.94-8.82×10 ⁻³ 0-3.4×10 ⁻⁷	Light-duty diesel vehicles (Uhrner et al., 2007) Light-duty gasoline vehicles (Seigneur, 2009)	6.25×10 ⁻⁵
H ₂ O	99	Light-duty diesel vehicles (Uhrner et al., 2007)	99
BC	0.0063	SP2 data (Liggio et al., 2012)	0.0063
Non-volatile POA	0.0020	MOBILE6.2C	0.0020

4

5

1

Table 5. Particle number-size distribution parameters assumed by the model.

Sampling site	Particle mode	Number concentration (#/cm³)	Geometric mean diameter(nm)	σ
Background	Soot mode	5000	50	1.6
	Accumulation mode	800	120	1.6
Tailpipe (raw exhaust)	Nucleation mode	3.86×10^7	15	1.4
	Soot mode	9.42×10^6	60	1.6

2

3

1

2

3 Table 6. Number concentration and mean diameter of the nucleation mode particles
 4 predicted by the model under different scenarios. *Normalized bias (in percentage) was

5 calculated as $(\text{base case} - \text{scenario})/\text{base case} \times 100\%$.

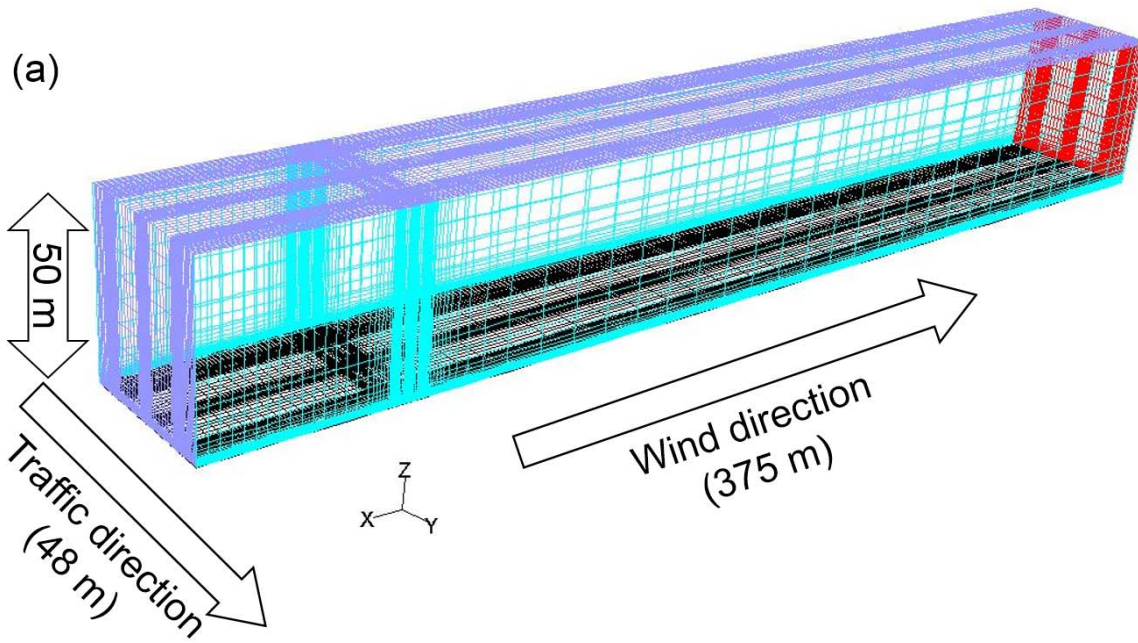
	Sampling site	Base case	Without deposition	Without condensation	Without nucleation	Without coagulation
Number concentration (#/cm ³)	B	5.94×10 ⁴ (N/A)	7.29×10 ⁴ (-23%)*	6.29×10 ³ (89%)	3.77×10 ⁴ (36%)	5.79×10 ⁴ (2%)
	C	1.59×10 ⁴ (N/A)	2.44×10 ⁴ (-53%)	9.63×10 ² (94%)	1.42×10 ⁴ (10%)	1.64×10 ⁴ (-3%)
Geometric-mean diameter (nm)	B	19.8	18.8	15.5	20.2	19.5
	C	24.3	19.6	15.2	25.4	23.3

6

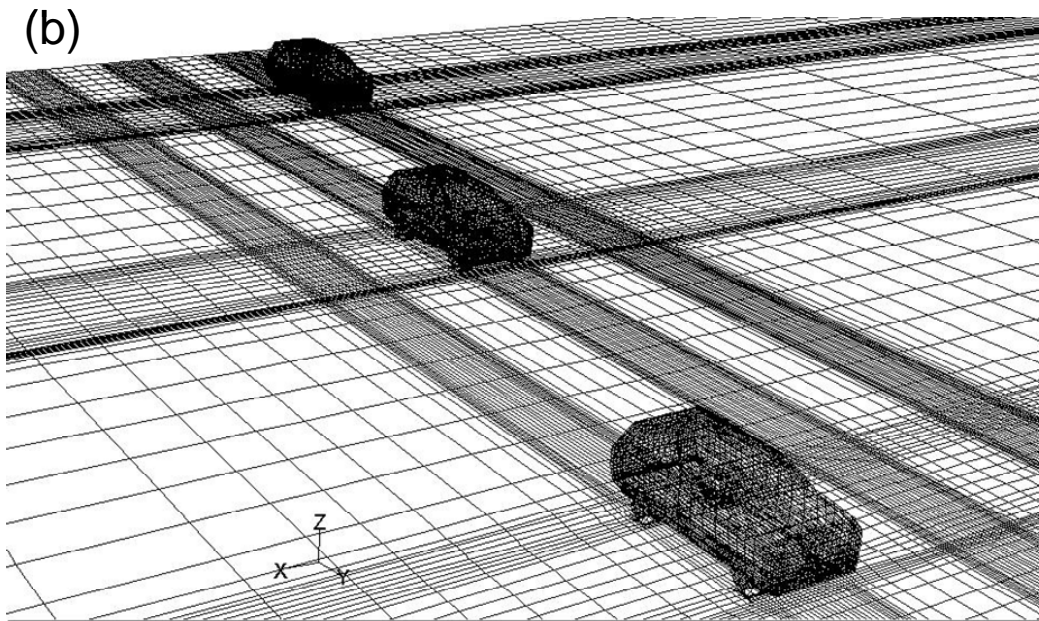
7

8

1



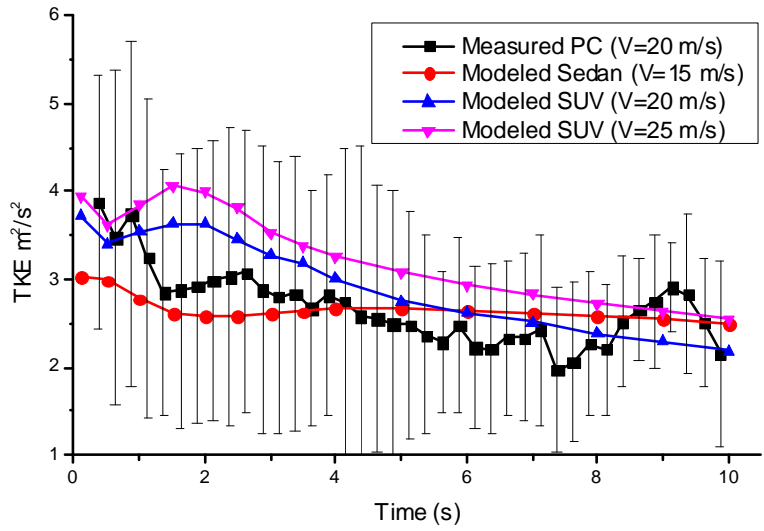
2



3

4 Fig. 1. Computational domain (a) and running vehicles and ground mesh (b). Purple mesh
5 indicates velocity-inlet boundaries (left and top); Red mesh indicates pressure-outlet
6 boundary (right); Black mesh indicates wall boundaries (bottom and cars); and cyan mesh
7 indicates translational periodic boundaries (lateral).

1

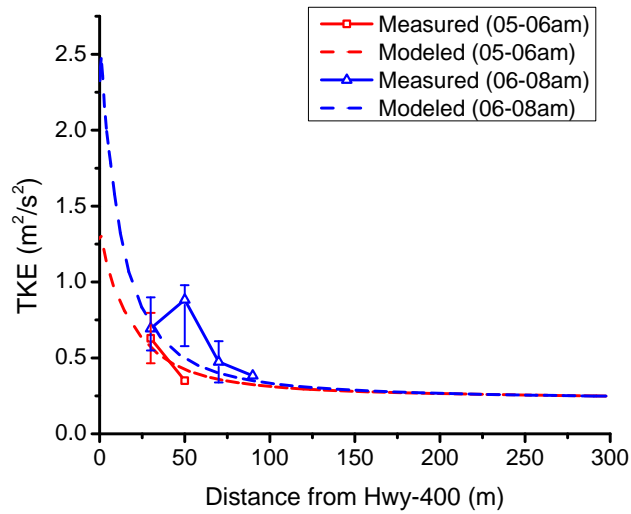


2

3 Fig. 2. Comparison of the on-road TKE from the passenger vehicle chasing experiments
4 of the FEVER project (black line) and model simulations (red, blue and purple lines). The
5 error bars represent the 25th and 75th percentiles of the measured on-road TKE. PC stands
6 for passenger vehicle and SUV stands for sport utility vehicle. V is the average travelling
7 speed (m/s) of PC in chasing experiments or the vehicle speed used in model simulation.

8

9



1

2 Fig. 3. Comparison of the TKE from the FEVER observations at a roadside tower and

3 model simulations for morning rush hours: 05:00-06:00 (red) and 06:00-08:00 a.m.

4 (blue). Measurement data are plotted in solid lines and model simulation results are

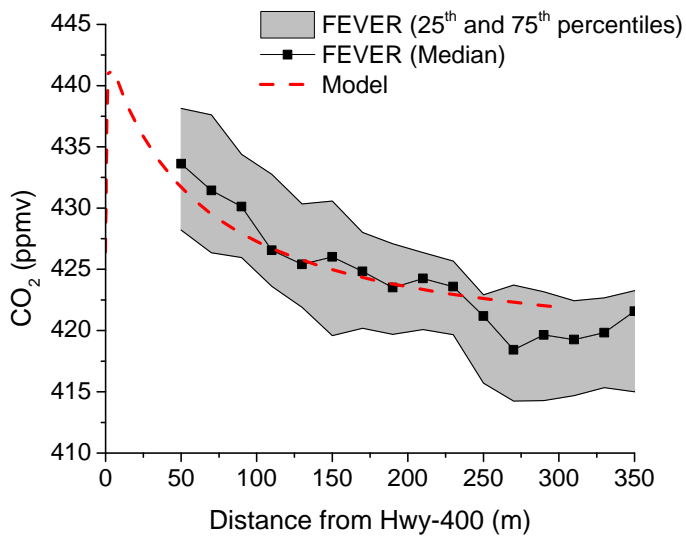
5 plotted in dashed lines. The error bars on top of measurement data represent 25th to 75th

6 percentiles.

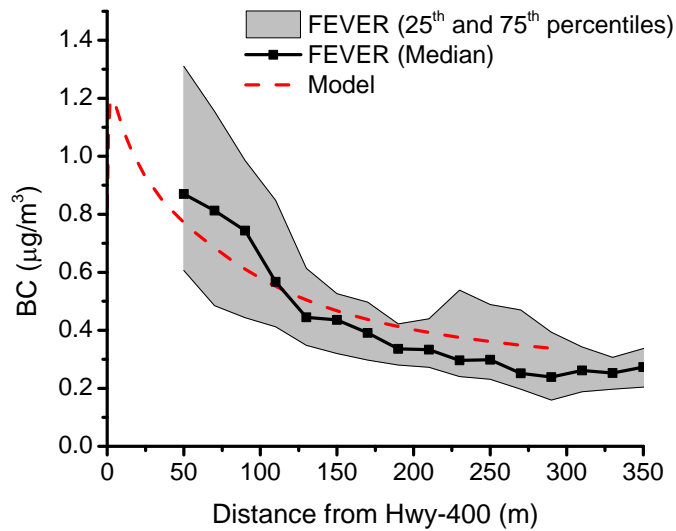
7

8

1



2



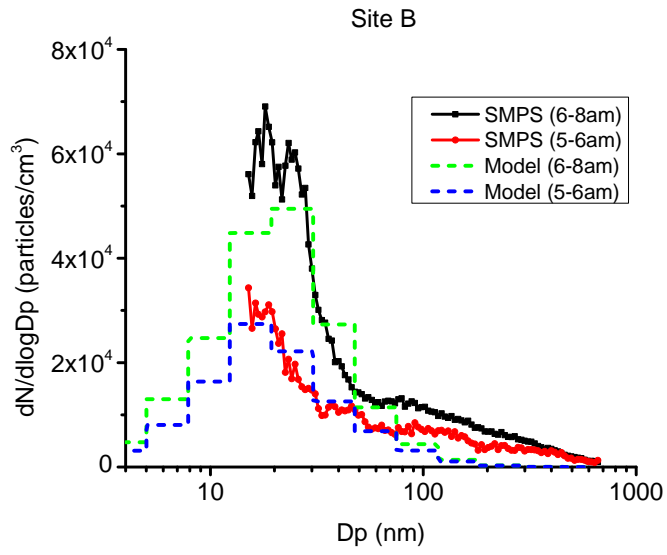
3

4 Fig. 4. Comparison of modelled and measured near-road concentrations of CO₂ (ppmv)
5 and BC (µg/m³) on the downwind side of Hwy-400. Median concentrations from FEVER
6 measurements are plotted in black solid lines, and modelled concentrations are plotted in
7 red dashed lines. The grey areas represent measurements within 25th and 75th percentiles.

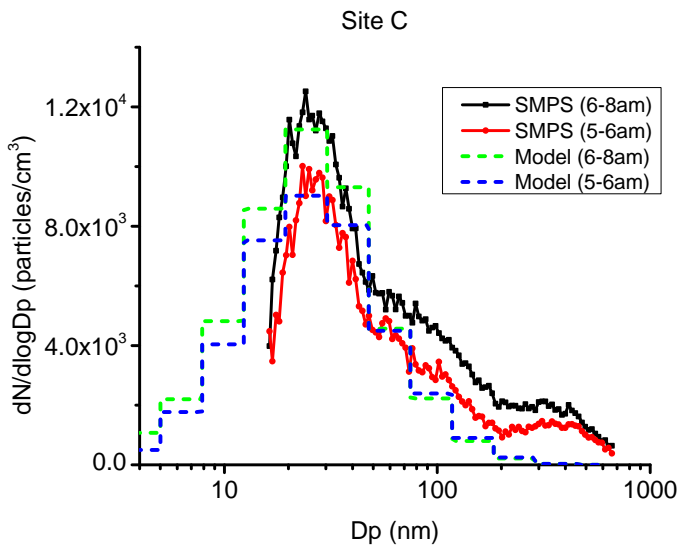
8

1

2



3



4

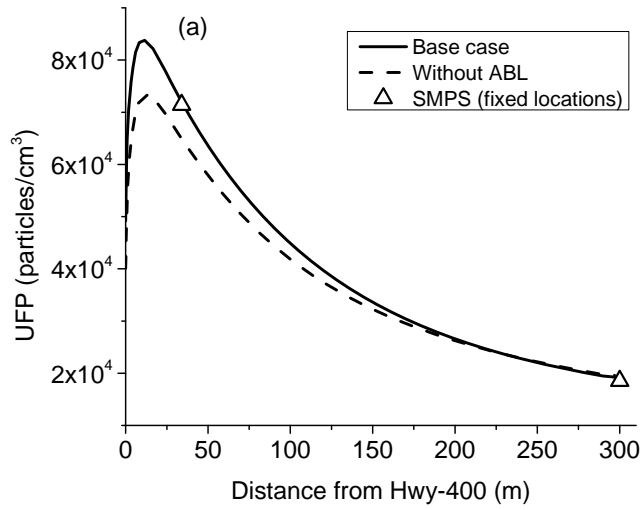
5 Fig. 5. Particle number-size distributions at site B (34 m from the hwy centre) and site C

6 (300 m from the hwy centre).

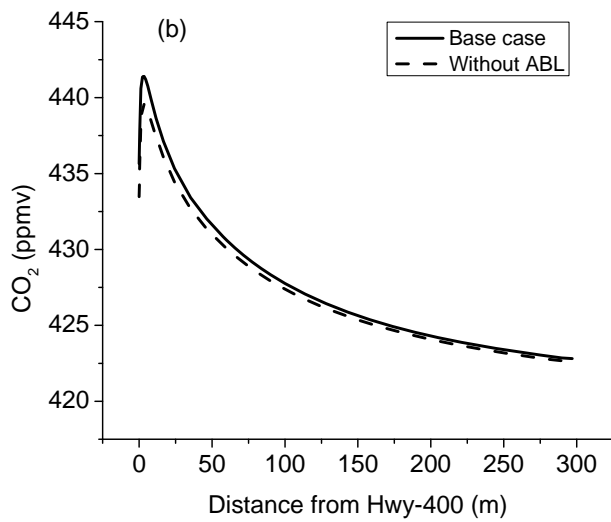
7

8

1



2



3

4 Fig. 6. Predicted UFP number (a) and CO₂ (b) concentrations as a function of distance to
5 the centre of Hwy-400.

1

2 **Reference**

- 3 Albriet, B., Sartelet, K. N., Lacour, S., Carissimo, B., and Seigneur, C.: Modelling
4 aerosol number distributions from a vehicle exhaust with an aerosol CFD model,
5 *Atmos. Environ.*, 44, 1126-1137, 10.1016/j.atmosenv.2009.11.025, 2010.
- 6 Alinot, C., and Masson, C.: k-epsilon Model for the atmospheric boundary layer under
7 various thermal stratifications, *J. Sol. Energy Eng. Trans.-ASME*, 127, 438-443,
8 10.1115/1.2035704, 2005.
- 9 Arnold, F., Pirjola, L., Aufmhoff, H., Schuck, T., Lahde, T., and Hameri, K.: First
10 gaseous sulfuric acid measurements in automobile exhaust: Implications for volatile
11 nanoparticle formation, *Atmos. Environ.*, 40, 7097-7105,
12 10.1016/j.atmosenv.2006.06.038, 2006.
- 13 Balogh, M., Parente, A., and Benocci, C.: RANS simulation of ABL flow over complex
14 terrains applying an Enhanced k-epsilon model and wall function formulation:
15 Implementation and comparison for fluent and OpenFOAM, *J. Wind Eng. Ind.*
16 *Aerodyn.*, 104, 360-368, 10.1016/j.jweia.2012.02.023, 2012.
- 17 Beckerman, B., Jerrett, M., Brook, J. R., Verma, D. K., Arain, M. A., and Finkelstein, M.
18 M.: Correlation of nitrogen dioxide with other traffic pollutants near a major
19 expressway, *Atmos. Environ.*, 42, 275-290, 10.1016/j.atmosenv.2007.09.042, 2008.
- 20 Blocken, B., Carmeliet, J., and Stathopoulos, T.: CFD evaluation of wind speed
21 conditions in passages between parallel buildings - effect of wall-function roughness
22 modifications for the atmospheric boundary layer flow, *J. Wind Eng. Ind. Aerodyn.*,
23 95, 941-962, 10.1016/j.jweia.2007.01.013, 2007a.
- 24 Blocken, B., Stathopoulos, T., and Carmeliet, J.: CFD simulation of the atmospheric
25 boundary layer: wall function problems, *Atmos. Environ.*, 41, 238-252,
26 10.1016/j.atmosenv.2006.08.019, 2007b.
- 27 Brugge, D., Durant, J. L., and Rioux, C.: Near-highway pollutants in motor vehicle
28 exhaust: A review of epidemiologic evidence of cardiac and pulmonary health risks,
29 *Environ. Health*, 6, 12, 10.1186/1476-069x-6-23, 2007.
- 30 Carpentieri, M., Kumar, P., and Robins, A.: An overview of experimental results and
31 dispersion modelling of nanoparticles in the wake of moving vehicles, *Environ.*
32 *Pollut.*, 159, 685-693, 10.1016/j.envpol.2010.11.041, 2011.
- 33 Chan, T. L., Liu, Y. H., and Chan, C. K.: Direct quadrature method of moments for the
34 exhaust particle formation and evolution in the wake of the studied ground vehicle, *J.*
35 *Aerosol. Sci.*, 41, 553-568, 10.1016/j.jaerosci.2010.03.005, 2010.
- 36 Clements, A. L., Jia, Y. L., Denbleyker, A., McDonald-Buller, E., Fraser, M. P., Allen,
37 D. T., Collins, D. R., Michel, E., Pudota, J., Sullivan, D., and Zhu, Y. F.: Air
38 pollutant concentrations near three Texas roadways, part II: Chemical
39 characterization and transformation of pollutants, *Atmos. Environ.*, 43, 4523-4534,
40 10.1016/j.atmosenv.2009.06.044, 2009.
- 41 Dahl, A., Gharibi, A., Swietlicki, E., Gudmundsson, A., Bohgard, M., Ljungman, A.,
42 Blomqvist, G., and Gustafsson, M.: Traffic-generated emissions of ultrafine particles
43 from pavement-tire interface, *Atmos. Environ.*, 40, 1314-1323,
44 10.1016/j.atmosenv.2005.10.029, 2006.

1 Di Sabatino, S., Buccolieri, R., Pulvirenti, B., and Britter, R.: Simulations of pollutant
2 dispersion within idealised urban-type geometries with CFD and integral models,
3 *Atmos. Environ.*, 41, 8316-8329, 10.1016/j.atmosenv.2007.06.052, 2007.

4 Franke, J.: Best practice guideline for the CFD simulation of flows in the urban
5 environment, Meteorological Inst., 2007.

6 Gidhagen, L., Johansson, C., Strom, J., Kristensson, A., Swietlicki, E., Pirjola, L., and
7 Hansson, H. C.: Model simulation of ultrafine particles inside a road tunnel, *Atmos.*
8 *Environ.*, 37, 2023-2036, 10.1016/s1352-2310(03)00124-9, 2003.

9 Gidhagen, L., Johansson, C., Langner, J., and Olivares, G.: Simulation of NOx and
10 ultrafine particles in a street canyon in Stockholm, Sweden, *Atmos. Environ.*, 38,
11 2029-2044, 10.1016/j.atmosenv.2004.02.014, 2004a.

12 Gidhagen, L., Johansson, C., Omstedt, G., Langner, J., and Olivares, G.: Model
13 simulations of NOx and ultrafine particles close to a Swedish highway, *Environ. Sci.*
14 *Technol.*, 38, 6730-6740, 10.1021/es0498134, 2004b.

15 Gong, S. L., Barrie, L. A., Blanchet, J. P., von Salzen, K., Lohmann, U., Lesins, G.,
16 Spacek, L., Zhang, L. M., Girard, E., Lin, H., Leitch, R., Leighton, H., Chylek, P.,
17 and Huang, P.: Canadian Aerosol Module: A size-segregated simulation of
18 atmospheric aerosol processes for climate and air quality models - 1. Module
19 development, *J. Geophys. Res.-Atmos.*, 108, 16, 10.1029/2001jd002002, 2003.

20 Gordon, M., Staebler, R. M., Liggio, J., Li, S.-M., Wentzell, J., Lu, G., Lee, P., and
21 Brook, J. R.: Measured and modeled variation in pollutant concentration near
22 roadways, *Atmos. Environ.*, 57, 10.1016/j.atmosenv.2012.04.022, 2012a.

23 Gordon, M., Staebler, R. M., Liggio, J., Makar, P., Li, S.-M., Wentzell, J., Lu, G., Lee,
24 P., and Brook, J. R.: Measurements of Enhanced Turbulent Mixing near Highways,
25 *Journal of Applied Meteorology and Climatology*, 51, 10.1175/jamc-d-11-0190.1,
26 2012b.

27 Gorle, C., van Beeck, J., Rarnbaud, P., and Van Tendeloo, G.: CFD modelling of small
28 particle dispersion: The influence of the turbulence kinetic energy in the atmospheric
29 boundary layer, *Atmos. Environ.*, 43, 673-681, 10.1016/j.atmosenv.2008.09.060,
30 2009.

31 Grahame, T. J.: Does improved exposure information for PM2.5 constituents explain
32 differing results among epidemiological studies?, *Inhal. Toxicol.*, 21, 381-393,
33 10.1080/08958370802380495, 2009.

34 Gustafsson, M., Blomquist, G., Gudmundsson, A., Dahl, A., Swietlicki, E., Bohyard, M.,
35 Lindbom, J., and Ljungman, A.: Properties and toxicological effects of particles from
36 the interaction between tyres, road pavement and winter traction material, *Sci. Total*
37 *Environ.*, 393, 226-240, 10.1016/j.scitotenv.2007.12.030, 2008.

38 Hagler, G. S. W., Tang, W., Freeman, M. J., Heist, D. K., Perry, S. G., and Vette, A. F.:
39 Model evaluation of roadside barrier impact on near-road air pollution, *Atmos.*
40 *Environ.*, 45, 2522-2530, 10.1016/j.atmosenv.2011.02.030, 2011.

41 Hargreaves, D. M., and Wright, N. G.: On the use of the k-epsilon model in commercial
42 CFD software to model the neutral atmospheric boundary layer, *J. Wind Eng. Ind.*
43 *Aerodyn.*, 95, 355-369, 10.1016/j.jweia.2006.08.002, 2007.

44 Jacobson, M. Z.: *Fundamentals of atmospheric modeling*, Cambridge University Press,
45 2005.

1 Karner, A. A., Eisinger, D. S., and Niemeier, D. A.: Near-Roadway Air Quality:
2 Synthesizing the Findings from Real-World Data, *Environ. Sci. Technol.*, 44, 5334-
3 5344, 10.1021/es100008x, 2010.

4 Keskinen, J., and Ronkko, T.: Can Real-World Diesel Exhaust Particle Size Distribution
5 be Reproduced in the Laboratory? A Critical Review, *J. Air Waste Manage. Assoc.*,
6 60, 1245-1255, 10.3155/1047-3289.60.10.1245, 2010.

7 Ketzel, M., and Berkowicz, R.: Modelling the fate of ultrafine particles from exhaust pipe
8 to rural background: an analysis of time scales for dilution, coagulation and
9 deposition, *Atmos. Environ.*, 38, 2639-2652, 10.1016/j.atmosenv.2004.02.020, 2004.

10 Kim, D. H., Gautam, M., and Gera, D.: On the prediction of concentration variations in a
11 dispersing heavy-duty truck exhaust plume using k-epsilon turbulent closure, *Atmos.*
12 *Environ.*, 35, 5267-5275, 10.1016/s1352-2310(01)00339-9, 2001.

13 Kirchner, U., Scheer, V., Vogt, R., and Kagi, R.: TEM study on volatility and potential
14 presence of solid cores in nucleation mode particles from diesel powered passenger
15 cars, *J. Aerosol. Sci.*, 40, 55-64, 10.1016/j.jaerosci.2008.08.002, 2009.

16 Kuhn, T., Biswas, S., and Sioutas, C.: Diurnal and seasonal characteristics of particle
17 volatility and chemical composition in the vicinity of a light-duty vehicle freeway,
18 *Atmos. Environ.*, 39, 7154-7166, 10.1016/j.atmosenv.2005.08.025, 2005.

19 Kulmala, M., Riipinen, I., Sipila, M., Manninen, H. E., Petaja, T., Junninen, H., Dal
20 Maso, M., Mordas, G., Mirme, A., Vana, M., Hirsikko, A., Laakso, L., Harrison, R.
21 M., Hanson, I., Leung, C., Lehtinen, K. E. J., and Kerminen, V. M.: Toward direct
22 measurement of atmospheric nucleation, *Science*, 318, 89-92,
23 10.1126/science.1144124, 2007.

24 Kumar, P., Fennell, P., Langley, D., and Britter, R.: Pseudo-simultaneous measurements
25 for the vertical variation of coarse, fine and ultrafine particles in an urban street
26 canyon, *Atmos. Environ.*, 42, 4304-4319, 10.1016/j.atmosenv.2008.01.010, 2008.

27 Kumar, P., Garmory, A., Ketzel, M., Berkowicz, R., and Britter, R.: Comparative study
28 of measured and modelled number concentrations of nanoparticles in an urban street
29 canyon, *Atmos. Environ.*, 43, 949-958, 10.1016/j.atmosenv.2008.10.025, 2009.

30 Kumar, P., Pirjola, L., Ketzel, M., and Harrison, R. M.: Nanoparticle emissions from 11
31 non-vehicle exhaust sources - A review, *Atmos. Environ.*, 67, 252-277,
32 10.1016/j.atmosenv.2012.11.011, 2013.

33 Labovsky, J., and Jelemensky, L.: Verification of CFD pollution dispersion modelling
34 based on experimental data, *J. Loss Prev. Process Ind.*, 24, 166-177,
35 10.1016/j.jlp.2010.12.005, 2011.

36 Li, L., Li, X. F., Lin, B. R., and Zhu, Y. X.: Improved k-epsilon two-equation turbulence
37 model for canopy flow, *Atmos. Environ.*, 40, 762-770,
38 10.1016/j.atmosenv.2005.10.010, 2006a.

39 Li, X. X., Liu, C. H., Leung, D. Y. C., and Lam, K. M.: Recent progress in CFD
40 modelling of wind field and pollutant transport in street canyons, *Atmos. Environ.*,
41 40, 5640-5658, 10.1016/j.atmosenv.2006.04.055, 2006b.

42 Liggio, J., Gordon, M., Smallwood, G., Li, S.-M., Stroud, C., Staebler, R., Lu, G., Lee,
43 P., Taylor, B., and Brook, J. R.: Are Emissions of Black Carbon from Gasoline
44 Vehicles Underestimated? Insights from Near and On-Road Measurements, *Environ.*
45 *Sci. Technol.*, 46, 10.1021/es2033845, 2012.

- 1 Mathis, U., Ristimäki, J., Mohr, M., Keskinen, J., Ntziachristos, L., Samaras, Z., and
2 Mikkanen, P.: Sampling conditions for the measurement of nucleation mode particles
3 in the exhaust of a diesel vehicle, *Aerosol Sci. Technol.*, 38, 1149-1160,
4 10.1080/027868290891497, 2004.
- 5 Mathissen, M., Scheer, V., Vogt, R., and Benter, T.: Investigation on the potential
6 generation of ultrafine particles from the tire-road interface, *Atmos. Environ.*, 45,
7 6172-6179, 10.1016/j.atmosenv.2011.08.032, 2011.
- 8 Nikolova, I., Janssen, S., Vos, P., Vrancken, K., Mishra, V., and Berghmans, P.:
9 Dispersion modelling of traffic induced ultrafine particles in a street canyon in
10 Antwerp, Belgium and comparison with observations, *Sci. Total Environ.*, 412, 336-
11 343, 10.1016/j.scitotenv.2011.09.081, 2011a.
- 12 Nikolova, I., Janssen, S., Vrancken, K., Vos, P., Mishra, V., and Berghmans, P.: Size
13 resolved ultrafine particles emission model - A continuous size distribution approach,
14 *Sci. Total Environ.*, 409, 3492-3499, 10.1016/j.scitotenv.2011.05.015, 2011b.
- 15 Ning, Z., Hu, N., Daher, N., Kam, W., Herner, J., Kozawa, K., Mara, S., and Sioutas,
16 C.: Impact of roadside noise barriers on particle size distributions and pollutants
17 concentrations near freeways, *Atmos. Environ.*, 44, 3118-3127,
18 10.1016/j.atmosenv.2010.05.033, 2010.
- 19 Pant, P., and Harrison, R. M.: Estimation of the contribution of road traffic emissions to
20 particulate matter concentrations from field measurements: A review, *Atmos.*
21 *Environ.*, 77, 78-97, 10.1016/j.atmosenv.2013.04.028, 2013.
- 22 Parente, A., Gorle, C., van Beeck, J., and Benocci, C.: A Comprehensive Modelling
23 Approach for the Neutral Atmospheric Boundary Layer: Consistent Inflow
24 Conditions, Wall Function and Turbulence Model, *Bound.-Layer Meteor.*, 140, 411-
25 428, 10.1007/s10546-011-9621-5, 2011a.
- 26 Parente, A., Gorle, C., van Beeck, J., and Benocci, C.: Improved kappa-epsilon model
27 and wall function formulation for the RANS simulation of ABL flows, *J. Wind Eng.*
28 *Ind. Aerodyn.*, 99, 267-278, 10.1016/j.jweia.2010.12.017, 2011b.
- 29 Petroff, A., and Zhang, L.: Development and validation of a size-resolved particle dry
30 deposition scheme for application in aerosol transport models, *Geosci. Model Dev.*, 3,
31 753-769, 10.5194/gmd-3-753-2010, 2010.
- 32 Pirjola, L., Paasonen, P., Pfeiffer, D., Hussein, T., Hameri, K., Koskentalo, T., Virtanen,
33 A., Ronkko, T., Keskinen, J., Pakkanen, T. A., and Hillamo, R. E.: Dispersion of
34 particles and trace gases nearby a city highway: Mobile laboratory measurements in
35 Finland, *Atmos. Environ.*, 40, 867-879, 10.1016/j.atmosenv.2005.10.018, 2006.
- 36 Pontiggia, M., Derudi, M., Busini, V., and Rota, R.: Hazardous gas dispersion: A CFD
37 model accounting for atmospheric stability classes, *J. Hazard. Mater.*, 171, 739-747,
38 10.1016/j.jhazmat.2009.06.064, 2009.
- 39 Pye, H. O. T., and Seinfeld, J. H.: A global perspective on aerosol from low-volatility
40 organic compounds, *Atmos. Chem. Phys.*, 10, 4377-4401, 10.5194/acp-10-4377-
41 2010, 2010.
- 42 Reponen, T., Grinshpun, S. A., Trakumas, S., Martuzevicius, D., Wang, Z. M.,
43 LeMasters, G., Lockey, J. E., and Biswas, P.: Concentration gradient patterns of
44 aerosol particles near interstate highways in the Greater Cincinnati airshed, *J.*
45 *Environ. Monit.*, 5, 557-562, 10.1039/b303557c, 2003.

- 1 Richards, P. J., and Hoxey, R. P.: APPROPRIATE BOUNDARY-CONDITIONS FOR
2 COMPUTATIONAL WIND ENGINEERING MODELS USING THE KAPPA-
3 EPSILON TURBULENCE MODEL, *J. Wind Eng. Ind. Aerodyn.*, 46-7, 145-153,
4 10.1016/0167-6105(93)90124-7, 1993.
- 5 Riddle, A., Carruthers, D., Sharpe, A., McHugh, C., and Stocker, J.: Comparisons
6 between FLUENT and ADMS for atmospheric dispersion modelling, *Atmospheric*
7 *Environment*, 38, 1029-1038, 10.1016/j.atmosenv.2003.10.052, 2004.
- 8 Rodi, W.: Comparison of LES and RANS calculations of the flow around bluff bodies, *J.*
9 *Wind Eng. Ind. Aerodyn.*, 71, 55-75, 1997.
- 10 Ronkko, T., Virtanen, A., Kannosto, J., Keskinen, J., Lappi, M., and Pirjola, L.:
11 Nucleation mode particles with a nonvolatile core in the exhaust of a heavy duty
12 diesel vehicle, *Environ. Sci. Technol.*, 41, 6384-6389, 10.1021/es0705339, 2007.
- 13 Ruckerl, R., Phipps, R. P., Schneider, A., Frampton, M., Cyrus, J., Oberdorster, G.,
14 Wichmann, H. E., and Peters, A.: Ultrafine particles and platelet activation in patients
15 with coronary heart disease—results from a prospective panel study, *Part Fibre*
16 *Toxicol.*, 4, 1743-8977, 2007.
- 17 Schlesinger, R. B.: The health impact of common inorganic components of fine
18 particulate matter (PM_{2.5}) in ambient air: A critical review, *Inhal. Toxicol.*, 19, 811-
19 832, 10.1080/08958370701402382, 2007.
- 20 Seigneur, C.: Current Understanding of Ultrafine Particulate Matter Emitted from Mobile
21 Sources, *J. Air Waste Manage. Assoc.*, 59, 3-17, 10.3155/1047-3289.59.1.3, 2009.
- 22 Sklavounos, S., and Rigas, F.: Validation of turbulence models in heavy gas dispersion
23 over obstacles, *J. Hazard. Mater.*, 108, 9-20, 10.1016/j.jhazmat.2004.01.005, 2004.
- 24 Stroud, C. A., Liggio, J., Zhang, J., Gordon, M., Staebler, R. M., Makar, P. A., Zhang, J.,
25 Li, S. M., Mihele, C., and Lu, G.: Rapid Organic Aerosol Formation Downwind of a
26 Highway: Measured and Model Results from the FEVER study, *Journal of*
27 *Geophysical Research: Atmospheres*, 2014.
- 28 Tominaga, Y., and Stathopoulos, T.: Turbulent Schmidt numbers for CFD analysis with
29 various types of flowfield, *Atmos. Environ.*, 41, 8091-8099,
30 10.1016/j.atmosenv.2007.06.054, 2007.
- 31 Toner, S. M., Shields, L. G., Sodeman, D. A., and Prather, K. A.: Using mass spectral
32 source signatures to apportion exhaust particles from gasoline and diesel powered
33 vehicles in a freeway study using UF-ATOFMS, *Atmos. Environ.*, 42, 568-581,
34 10.1016/j.atmosenv.2007.08.005, 2008.
- 35 Uhrner, U., von Lowis, S., Vehkamäki, H., Wehner, B., Brasel, S., Hermann, M.,
36 Stratmann, F., Kulmala, M., and Wiedensohler, A.: Dilution and aerosol dynamics
37 within a diesel car exhaust plume - CFD simulations of on-road measurement
38 conditions, *Atmos. Environ.*, 41, 7440-7461, 10.1016/j.atmosenv.2007.05.057, 2007.
- 39 Uhrner, U., Zallinger, M., von Lowis, S., Vehkamäki, H., Wehner, B., Stratmann, F., and
40 Wiedensohler, A.: Volatile Nanoparticle Formation and Growth within a Diluting
41 Diesel Car Exhaust, *J. Air Waste Manage. Assoc.*, 61, 399-408, 10.3155/1047-
42 3289.61.4.399, 2011.
- 43 Valavanidis, A., Fiotakis, K., and Vlachogianni, T.: Airborne Particulate Matter and
44 Human Health: Toxicological Assessment and Importance of Size and Composition
45 of Particles for Oxidative Damage and Carcinogenic Mechanisms, *J. Environ. Sci.*

1 Health Pt. C-Environ. Carcinog. Ecotoxicol. Rev., 26, 339-362,
2 10.1080/10590500802494538, 2008.

3 Vehkamäki, H., Kulmala, M., Lehtinen, K. E. J., and Noppel, M.: Modelling binary
4 homogeneous nucleation of water-sulfuric acid vapours: Parameterisation for high
5 temperature emissions, Environ. Sci. Technol., 37, 3392-3398, 10.1021/es0263442,
6 2003.

7 Wang, Y. J., and Zhang, K. M.: Modeling Near-Road Air Quality Using a Computational
8 Fluid Dynamics Model, CFD-VIT-RIT, Environ. Sci. Technol., 43, 7778-7783,
9 10.1021/es9014844, 2009.

10 Wang, Y. J., and Zhang, K. M.: Coupled turbulence and aerosol dynamics modeling of
11 vehicle exhaust plumes using the CTAG model, Atmos. Environ., 59, 284-293,
12 10.1016/j.atmosenv.2012.04.062, 2012.

13 Wang, Y. J., Nguyen, M. T., Steffens, J. T., Tong, Z. M., Wang, Y. G., Hopke, P. K., and
14 Zhang, K. M.: Modeling multi-scale aerosol dynamics and micro-environmental air
15 quality near a large highway intersection using the CTAG model, Sci. Total Environ.,
16 443, 375-386, 10.1016/j.scitotenv.2012.10.102, 2013.

17 Xie, Z. T., and Castro, I. P.: Efficient generation of inflow conditions for large eddy
18 simulation of street-scale flows, Flow Turbul. Combust., 81, 449-470,
19 10.1007/s10494-008-9151-5, 2008.

20 Zhang, C. X.: NUMERICAL PREDICTIONS OF TURBULENT RECIRCULATING-
21 FLOWS WITH A KAPPA-EPSILON-MODEL, J. Wind Eng. Ind. Aerodyn., 51, 177-
22 201, 10.1016/0167-6105(94)90003-5, 1994.

23 Zhang, K. M., and Wexler, A. S.: Evolution of particle number distribution near
24 roadways - Part I: analysis of aerosol dynamics and its implications for engine
25 emission measurement, Atmos. Environ., 38, 6643-6653,
26 10.1016/j.atmosenv.2004.06.043, 2004.

27 Zhang, K. M., Wexler, A. S., Zhu, Y. F., Hinds, W. C., and Sioutas, C.: Evolution of
28 particle number distribution near roadways. Part II: the 'road-to-ambient' process,
29 Atmos. Environ., 38, 6655-6665, 10.1016/j.atmosenv.2004.06.044, 2004.

30 Zhang, L. M., Gong, S. L., Padro, J., and Barrie, L.: A size-segregated particle dry
31 deposition scheme for an atmospheric aerosol module, Atmos. Environ., 35, 549-560,
32 10.1016/s1352-2310(00)00326-5, 2001.

33 Zhou, Y., and Levy, J. I.: Factors influencing the spatial extent of mobile source air
34 pollution impacts: a meta-analysis, BMC Public Health, 7, 11, 10.1186/1471-2458-7-
35 89, 2007.

36 Zhu, Y. F., Hinds, W. C., Kim, S., Shen, S., and Sioutas, C.: Study of ultrafine particles
37 near a major highway with heavy-duty diesel traffic, Atmos. Environ., 36, 4323-4335,
38 10.1016/s1352-2310(02)00354-0, 2002a.

39 Zhu, Y. F., Hinds, W. C., Kim, S., and Sioutas, C.: Concentration and size distribution of
40 ultrafine particles near a major highway, J. Air Waste Manage. Assoc., 52, 1032-
41 1042, 2002b.

42 Zhu, Y. F., Pudota, J., Collins, D., Allen, D., Clements, A., DenBleyker, A., Fraser, M.,
43 Jia, Y. L., McDonald-Buller, E., and Michel, E.: Air pollutant concentrations near
44 three Texas roadways, Part I: Ultrafine particles, Atmos. Environ., 43, 4513-4522,
45 10.1016/j.atmosenv.2009.04.018, 2009.

46